RESEARCH ARTICLE | DECEMBER 17 2019

A CHT framework for the CFD analysis of the spray-wall thermal interaction in the dosing unit of SCR systems for diesel engines FREE

Antonello Nappi; Gianluca Montenegro; Angelo Onorati; Augusto Della Torre

AIP Conf. Proc. 2191, 020118 (2019)
https://doi.org/10.1063/1.5138851

A CHT Framework For The CFD Analysis Of The Spray-Wall Thermal Interaction In The Dosing Unit Of SCR Systems For Diesel Engines

Antonello Nappi[1,a)], Gianluca Montenegro[1,b)], Angelo Onorati[1,c)] and Augusto Della Torre[1,d)]

[1]*Dipartimento di Energia, Politecnico di Milano, Milano, Italy.*

[a)]antonello.nappi@polimi.it
[b)]gianluca.montenegro@polimi.it
[c)]angelo.onorati@polimi.it
[d)]augusto.dellatorre@polimi.it

Abstract. In this work, a Conjugate Heat Transfer (CHT) framework for the simulation of the full kinematic and thermal interaction of the spray with the walls has been implemented and applied to a test case. Full coupling between the gaseous, spray and liquid film were achieved, allowing to capture the full range of kinematic and thermal interactions between the spray, the wall and the liquid film (both in dry and wet conditions). The evolution of the film is handled through a multi component film model, with a coupling to the gaseous and solid phase. In particular, the coupling of the film with a CHT model of the solid wall allows the designer to have a comprehensive evaluation of the wall temperature evolution. To complete the description of the film evolution, a stripping model for droplets from the film is used, allowing the transfer of mass from the film surface to the lagrangian phase.

INTRODUCTION

In the last decade, selective catalytic reduction (SCR) has confirmed its role as the most cost-effective strategy for NOx reduction in Diesel engines. To perform its function, the SCR system requires a supply of ammonia, that is used as a reducing agent. As the storage of pure ammonia is not viable due to safety concerns, ammonia is supplied to the SCR in the form of a urea water solution (UWS), that is injected in the exhaust gas stream before the catalyst, where it undergoes evaporation and thermal decomposition. These processes lead to the formation of ammonia and isocyanic acid, assuming that the thermal decomposition process takes place after the complete evaporation of water. Furthermore, the hydrolysis of isocyanic acid in the exhaust gases leads to the formation of further ammonia, with an additional release of carbon dioxide. After these processes, the ammonia formed must be fed to the catalyst, ensuring the most uniform distribution to achieve the maximum NOx conversion efficiency. The application of this technology suffers from the limited time available to complete the evaporation of the spray. To ensure a complete conversion before the catalyst inlet, the performance of urea decomposition is usually improved by the interaction between the spray of UWS and the exhaust walls, due to the high heat fluxes that occur during the contact between wall and droplets. This interaction, however, can lead to a rapid cooling of the exhaust wall and to the consequent formation of a liquid film. The formation of this film must be avoided, as the reactions occurring inside it can lead to the formation of urea by-products responsible for the formation of solid deposits. A correct injection strategy (controlling the dosing and the timing of injection) becomes a key parameter to limit the formation of these deposits. In this scenario, the usage of CFD has become a fundamental step during the component design phase. To do so, a complete description of the spray behaviour is required, including the spray kinematic and thermal interaction with the wall. In this work, a model for the spray wall interaction has been implemented, capable of describing the full range of interactions between the spray and the walls, and the formation and evolution of a multi specie liquid film. This model was applied to a test case from the literature, and the results from the simulations were compared with experimental results in term of liquid film evolution. Finally, to show the capability of the model to capture the transition from hot to cold

74th ATI National Congress
AIP Conf. Proc. 2191, 020118-1–020118-11; https://doi.org/10.1063/1.5138851
Published by AIP Publishing. 978-0-7354-1938-4/$30.00

conditions, a simulation of a different configuration of the same test case was ran, with a wall temperature above the wetting threshold.

Governing equations

The CFD approach developed in this work is based on the formulation of conservation equations for compressible, unsteady and reacting flows. It is based on the Navier Stokes set of equations, with the addiction of the source terms due to the spray. Further details about these terms will be given in the next chapter.

Continuity equation

$$\frac{\partial \rho}{\partial t} + \nabla \cdot (\rho \mathbf{U}) = S_{m,p} \tag{1}$$

Momentum equation

$$\frac{\partial \rho \mathbf{U}}{\partial t} + \nabla \cdot (\rho \mathbf{U}\mathbf{U}) - \nabla \cdot [\mu(\nabla \mathbf{U} + (\nabla \mathbf{U})^T)] = \rho \mathbf{g} - \nabla \left(P + \frac{2}{3}\mu \nabla \cdot \mathbf{U} \right) + S_{u,p} \tag{2}$$

Energy equation

$$\frac{\partial \rho e}{\partial t} + \nabla \cdot (\rho e \mathbf{U}) - \nabla \cdot (\lambda \nabla T) = \rho \mathbf{g} \cdot \mathbf{U} - \nabla \cdot (P\mathbf{U}) - \nabla \cdot \left(\frac{2}{3}\mu (\nabla \cdot \mathbf{U})\mathbf{U} \right) + \nabla \cdot [\mu(\nabla \mathbf{U} + (\nabla \mathbf{U})^T) \cdot \mathbf{U}] + \rho Q + S_{e,p} \tag{3}$$

Species equation

$$\frac{\partial \rho Y_i}{\partial t} + \nabla \cdot (\rho Y_i \mathbf{U}) = -\nabla \cdot J_i + R_i + S_{i,p} \tag{4}$$

Where $S_{m,p}$, $S_{u,p}$, $S_{e,p}$ and $S_{i,p}$ are source terms that account for the interaction between the spray and the gas. The set of equations is then closed by the equations of state, and by the turbulence model. For the simulation presented here, the perfect gas model was used, while the turbulence model selected was the k-ϵ model.

Spray fundamental equations

The spray is modelled using a lagrangian approach, and is coupled with the eulerian phase by introducing appropriate terms inside the moementum, energy, mass and species conservation equations (sources in equations (1,2,3 and 4)). The spray properties are assigned to particles (parcels) that are followed in their spatial evolution from the initial position through their trajectory as they evolve. By using a statistical model, the tracking of the single droplets can be reduced to the tracking of a lower number of parcels (packages of droplets with the same properites), reducing the computational effort required. With this methodology, all the important phenomena involved in the spray evolution were included. In particular, the models used include:

1. Drag force between the spray and the gaseous phase.
2. Gravitational force.
3. Heat transfer between spray and the surrounding gases.
4. Evaporation of the spray.

The fundamental equations of this model will be now presented, starting with the mass equation.

Mass equation

The mass balance takes a very simple form for the model, as the droplets are considered to be spheres of diameter D. Calling C_{vap} the vaporization rate, the equations becomes:

$$\frac{dD^2}{dt} = C_{vap}. \tag{5}$$

If the same equation is written in term of mass variation of the droplets in time:

$$\dot{m_d} = -\pi \, D \, \Gamma \, \rho_v \, lnB \, Sh \tag{6}$$

where ρ_v is the vapour density close to the droplet, Γ is the mass diffusion coefficient, and Sh is the nondimensional Sherwood number. The Sherwood number takes into account the acceleration in the evaporation process due to the relative motion between gaseous and liquid phase, and is expressed as a function of the Reynolds and Schmidt number ($Sc = \frac{\mu}{\rho d}$):

$$Sh = 2 + 0.6\sqrt{Re}\sqrt[3]{Sc}. \tag{7}$$

And B is the Spalding number:

$$B = \frac{Y_{v,s} - Y_{v,\infty}}{1 - Y_{v,s}}. \tag{8}$$

The two equations (6, 8) are relevant when only vaporization is present. In the case of boiling, the saturation pressure tends to the ambient one, and $B \to \infty$, leading to an infinite vaporization rate. Thus in the boiling regime, the mass conservation equation must be corrected introducing a term to take into account that during boiling phase change is governed by heat exchange, and not diffusive phenomena.

Momentum equation

The momentum conservation equation is derived from the second law of dynamics:

$$\frac{d}{dt}(m_d u_d) = m_d \frac{du_d}{dt} = F \tag{9}$$

where m_d is the mass of the particle, u_d is the velocity of the particle, and F is the summation of the applied forces. In our case, F takes into account the drag and the gravity force (g):

$$F = -\frac{\pi D^2}{8}\rho C_d |u_d - u|(u_d - u) + m_g g. \tag{10}$$

In equation (10), C_d is the drag coefficient, and u is the velocity of the surrounding gas.

Energy equation

The droplets receive energy mainly from the surrounding gas phase, and are subjected to an increase in temperature and evaporate exploiting part of the energy received. This process continues until the gas around the particle reaches the saturation conditions. If the energy received is not enough, the droplets lose some internal energy, decreasing their temperature. The energy equation for the droplet can be therefore written as:

$$m_d \frac{dh_d}{dt} = \dot{m}_d h_l T_d + \pi D \lambda Nu (T - T_d) f \tag{11}$$

The vaporization rate $\dot{m}_d$ (negative) is the same term appearing in equation (6), the other terms represent the latent heat of vaporization ($h_l T_d$), the thermal conductivity of the gas (λ) and the Nusselt number (Nu). The Nusselt number represents the ratio between convective and conductive heat exchange, and is expressed as a function of the Reynolds and Prandtl number, using the Ranz and Marshall correlation [11]:

$$Nu = 2 + 0.6\sqrt{Re}\sqrt[3]{Pr}. \tag{12}$$

Notice that equation (12) is equivalent to (7), where the Schmidt number is substituted with the Prandtl number. This is because the mass exchange due to vaporization is closely linked to the heat exchange. Finally, the correction factor f takes into account the reduction in heat received because of the simultaneous transfer of mass to the gas phase:

$$f = \frac{z}{e^z - 1} \tag{13}$$

Where:

$$z = -\frac{c_{p,v}\dot{m}_d}{\pi d \lambda Nu} \tag{14}$$

To write this equation in a more useful form from the computational point of view, a heat transfer relaxation time τ_h can be written as:

$$\tau_h = \frac{m_d c_l}{\pi d \lambda Nu} \tag{15}$$

And equation (11) can be written as:

$$\frac{dT_d}{dt} = \frac{T - T_d}{\tau_h} f - \frac{1}{c_l} \frac{h_l T_d}{\tau_e} \tag{16}$$

On this framework, a model for the spray/wall kinematic and thermal interaction was added.

Spray wall interaction

Several models have been developed for the representation of the spray-wall interaction, depending on the parameters used for the classifications of the different impact regimes [2]. The model adopted in this work is based on is the one proposed by Kuhnke [6]. This model has been chosen because of its capability to characterise the kinematics of the spray impingement for a wide range of spray velocities and wall temperatures as it considers both the thermal and kinematic characteristics of the spray/wall interaction, using two parameters to distinguish between the different impact regimes:

1. The thermal parameter T^* is defined as the ratio between the wall temperature and the fluid saturation temperature $\frac{T_w}{T_{sat}}$.
2. The Kinematic parameter K is defined as $We^{\frac{5}{8}} La^{\frac{1}{8}}$

Where We (Weber number):

$$We = \frac{\rho v^2 l}{\sigma} \tag{17}$$

Describes the relative importance of inertial forces with respect to surface tension, and La (Laplace number):

$$La = \frac{\sigma \rho l}{\mu^2} \tag{18}$$

Represents the ratio between surface tension and viscous forces.
The whole impingement regime map is reported in Fig.(1), highlighting the critical values of the parameters K and T^*, and the different impact regimes. Since no clear influence of the impingement angle is found in literature, the

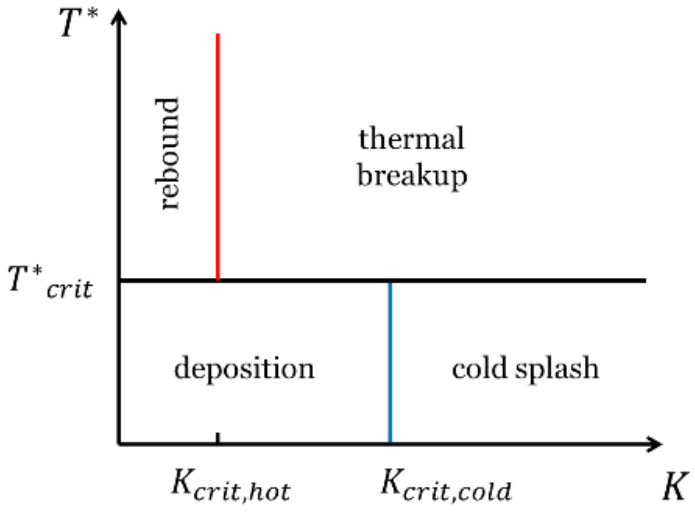

Figure 1. T^* K diagram, with different impact regimes

recognition of the impact regime is based on the normal component of the velocity (that appears in the We number), and therefore the kinematic parameter K is evaluated using the normal component of the velocity. To separate hot and cold wall behaviour a critical thermal parameter T^*_{crit} is set to 1.1 [10]; above this threshold, the temperature of the wall induces considerable breakup, reducing the kinematic threshold between conservative and destructive

impacts. When K is below the critical value, the parcel undergoes a rebound interaction, where a vapour layer between the droplet and wall is formed, preventing the direct contact and leading to the reflection of the impacting droplets, without the formation of a wall film. When the value of K goes over the critical value, droplets break up into secondary ones, again without the formation of a wall film. This impact regime is called thermal breakup.
Below the critical temperature, the deposition and splash interaction regimes are found. In the deposition regime the impacting droplet simply sticks to the wall, creating a wall film. In the splashing regime instead, particles are atomized and smaller secondary droplets form after the impact on the wall. In cold conditions the critical kinematic parameter is a complex function of the dimensionless temperature and of the wall roughness. In general, the critical kinematic parameter K increases with the temperature [9], (up to the hot wall thermal threshold), where the boiling induced breakup increases the probability of destructive interactions upon impact, and with roughness, since a rougher wall facilitates destructive interactions between droplet and wall. This effect of the roughness decreases with temperature, as the formation of a vapour cushion between the parcels and the wall reduces the interactions between parcels and wall crevices.
To determine the properties of the parcels after the interaction with the wall, several quantities need to be evaluated, such as mass fraction of the secondary drops, size ratio, velocity magnitude and direction, and the number of particle per parcels required to fulfil the overall mass balance. In the case a wall film is present, this ratio could be higher than 1, to allow for the removal of part of the liquid film by the impinging droplet. For a more in depth discussion of the model, the readed is referred to the works of Dominik Kuhnke [6], Bai and Gosman [2] and Nagaoka [8].
Regarding the thermal interaction between spray and wall, according to [12] the heat transfer between wall and droplets is well described with the assumption of contact between two semi-infinite bodies. With this approach, the energy balance can be formulated using the respective thermal effusivities b, computed as: $\sqrt{\rho\lambda c_p}$.

In this form, the energy exchanged can be written as:

$$Q = A_{con}\frac{2\sqrt{t_{con}}}{\sqrt{\pi}}\frac{b_w b}{b_w + b}(T_w - T). \tag{19}$$

Therefore, the energy exchanged is a function of wall temperature, effusivities, area and time of contact. The contact time is modelled as a function of the kinematic parameter, with two formulations, using $K = 40$ as delimiter [6].

$$t_{con} = \begin{cases} \sqrt{\frac{\pi}{2}}\left(\frac{pD^5}{\sigma U^2}\right)^{0.25} & \text{for } K \leq 40 \quad (20) \\ \frac{\pi}{4}\sqrt{\frac{pD^3}{\sigma}} & \text{for } K > 40 \quad (21) \end{cases}$$

The contact area instead is a function of the Weber number of the droplet, where the maximum diameter of the droplet is calculated as:

$$D_{con,max} = D\,0.61\,We^{0.38}. \tag{22}$$

The trend of the diameter with the contact time is assumed linear with the maximum at $t_{con}/2$ and then a reduction down to 0.

Liquid film modelling

In OpenFOAM, the formation and evolution of the wall film is made possible by defining specific solution fields on the patches where the formation of the liquid film is likely to occur. A number of scalar and vectorial fields are therefore defined, and the evolution of these fields is made possible by using the fundamental equations of fluid dynamics (conservation of mass, momentum, energy and species transport equations). Within this framework, a schematic representation of a thin liquid film on a curved surface can be represented using a single layered mesh, where it is possible to identify a curved wall surface S_w, with its normal n, a free surface of the liquid film S_{fs}, a liquid film of thickness h and an assumed velocity profile V, varying from zero at the wall to the free surface velocity V_{fs} (see Figure (2)).

A set of governing equations for the liquid film can be derived under the following assumptions:

- The thickness of the liquid film is small enough to apply a boundary layer approximation, implying that the gradients of all the quantities in the normal direction are much greater than the one in tangential direction;

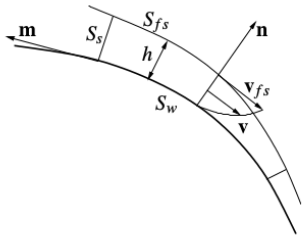

Figure 2. Liquid Film representation.

- The motion of the liquid film is caused by tangential gradients of the total pressure p_L, by momentum sources due to spray impingement, by shear at the interfaces, and by body forces such as the acceleration of gravity;
- The local pressure inside the liquid p_L can be considered as constant across the film thickness due to the boundary-layer approximation;
- The pressure p_L can be evaluated as the sum of different components: the pressure of the gas surrounding the film p_g, pressure due to capillary effects p_σ, hydrostatic pressure p_h and pressure due to spray impingement p_d; Thus, locally the film pressure can be written as:

$$p_L = p_g + p_d + p_\sigma + p_h. \tag{23}$$

- The source terms in the mass conservation equation due to impinging droplets can be considered as a smooth function, allowing the use of conventional differential operations.

Continuity equation

The film continuity equation can be written as a function of the film thickness h by considering a single face area, under the assumption of incompressible fluid.

$$\frac{\partial h}{\partial t} + \nabla \cdot \left(h\mathbf{U}_f\right) = S_M + S_V. \tag{24}$$

Equation (24) contains two different source terms, S_M and S_V. The former takes into account the mass coming from the impingement of droplets (which depends on the impingement regime), and can be expressed as:

$$S_M = \frac{4\pi\rho_d}{3A\rho_f\Delta t}\sum_{i=1}^{N_d} r_i^3. \tag{25}$$

The latter instead is the term associated with the mass transfer due to the evaporation, due to both dynamic and thermal effects [5].

Species equation

Since in the case of UWS there are a number of chemical species involved, a set of N_{k-1} equations were added, where k is the number of chemical species considered.

$$\frac{\partial hY_{f,k}}{\partial t} + \nabla \cdot \left(h\mathbf{U}_f Y_{f,k}\right) = S_{M,k} + S_{V,k}. \tag{26}$$

The right hand side terms $S_{M,k}$ and $S_{V,k}$ are the equivalent of the terms S_M and S_V in the continuity equation, for the k-th species.

Energy equation

In the context of SCR systems, the evolution of the liquid film is controlled by different phenomena, such as the heat exchange between the film and the surrounding gases, the conductive heat exchange with the walls, and the energy contribution due to the impingement of the spray. The energy equation, can be written in terms of the specific enthalpy as:

$$\frac{\partial h H_{s,f}}{\partial t} + \nabla \cdot \left(h \mathbf{u}_f H_{s,f} \right) = j_g - j_w + S_H, \tag{27}$$

The first term on the right hand side j_g represents the heat flux from the gas. This term takes into account both the flux due to the temperature gradient and the contribution due to the evaporation, whereas j_w is the flux due to the conduction with the wall. This contribution is evaluated considering the normal temperature gradient between the wall and the film. To allow the evolution of the wall temperature in the regions where there is formation of the liquid film, a term inside the energy equation of the solid is included, to account for the heat flux from the liquid layer (or, in the case of its absence, the heat flux from the surrounding gases).

$$\rho_w c_w \frac{\partial T_w}{\partial t} - \lambda_{t,w} \nabla^2 T_w = \frac{j_{w/g} \rho_f}{\delta}. \tag{28}$$

This contribution is represented by the term $j_{w/g}$.

Momentum equation

The momentum equation for the liquid film can be written as:

$$\frac{\partial h \mathbf{U}_f}{\partial t} + \nabla \cdot \left(h \mathbf{U}_f \mathbf{U}_f \right) = -\frac{1}{\rho_f} \nabla \left(h p_l \right) + \tau_{fs} - \tau_w + h \mathbf{g}_t + \mathbf{S}_U. \tag{29}$$

Starting from the first, the terms on the right hand side represent the different causes of film motion:

- $\nabla_s p_L$ is the pressure gradient on the surface
- $\boldsymbol{\tau}_{fs}$ is the viscous force in the tangential direction at the free-surface of the film;
- $\boldsymbol{\tau}_w$ is the shear at the wall interface;
- $\mathbf{g}_t$ is the tangential component of the gravitational acceleration;
- $\mathbf{S}_U$ is the source term due to the impingement of the spray

As the impact of the droplets on the film is not always perpendicular, S_U must be decomposed into two different parts, taking into account the effect of the normal velocity component and of the tangential one. In particular, the normal component of the velocity contribution gives a pressure contribution, while the tangential component enters in the momentum equation as S_U:

$$\mathbf{S}_U = \frac{4 \pi \rho_d}{3 A \rho_f \Delta t} \sum_{i=1}^{N_d} r_i^3 \left(\mathbf{u}_i \cdot \underline{t} \right) \underline{t}. \tag{30}$$

Validation test case

As the main focus of this paper is the modelling of the liquid film formation and its interaction with the solid and gas phases, the first results here presented come from a case where the temperature of the wall and of the incoming gas are below the wetting thresold (T^* below 1.1). In particular, experimental results available in the literature [1] were used to validate the models used for the spray and wall film.
The geometry of the case is described in the figure (3). The testing apparatus consists of a filming surface, separating two channels, where mineral spirits are injected from the top and impinge on the surface of the filmer. For the cases here presented, the lower inlet is considered closed, as it was kept closed to provide optical access to the lower surface of the filmer. After the filmer, a large chamber is used to direct the air/vapour mixture to the exhaust.

To build the calculation grid, a cartesian mesh generation utility was used, namely the OpenFOAM meshing utility blockMesh. It allows the generation of a hexahedral mesh, with possible local refinement based on an octree approach. One of the main advantages of such approach is the low non orthogonality of the mesh generated. In

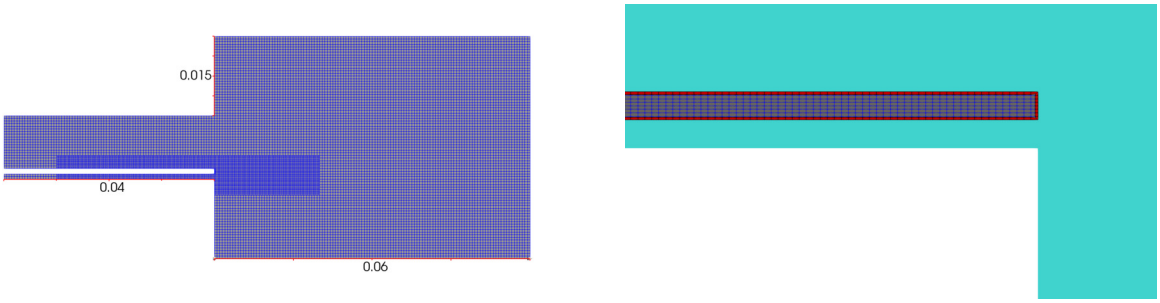

(a) (b)

Figure 3. The test case geometry: (a) Front view of the geometry, with the main dimensions. The inlet channel height is 1 cm, while the filmer thickness is 1 mm. (b) Detail of the film and solid meshes.

this hexahedral mesh, a refinement zone near the impact region of the spray was defined, to allow for a better film resolution and spray tracking near the filmer surface. Regarding the liquid film region, its mesh was generated by extruding the boundary where the liquid film formation is supposed to occur, generating a single layer mesh, which is treated by the solver as a two dimensional domain.
The solid mesh instead was generated by selecting a specific region in the generated mesh, and then applying a refinement in the thickness direction, to give a better resolution of the temperature gradient inside the solid wall. This approach was used to ensure the presence of a conformal interface between the gas, liquid film and solid region, required to allow the coupling between the three regions. In figure (3), a detail of the solid and film meshes can be seen, with the liquid film mesh highlighted in red. For further details about the mesh dimensions, cells number and simulation controls, see Table (1). Regarding the discretization schemes, for the solution of the fluid and liquid film first order schemes were used.

Simulation results

The results from the simulations performed are presented, starting from the cases with the same conditions as the literature cases, and then looking at the results of a hot case, suitably set to highlight the transition from dry to wet conditions.

In this work, two different conditions were simulated, with two different spray initial velocities, whose values are summarized in Table (1).

Table 1. Test case: details on BC, mesh and simulation controls.

	Case 1	**Case 2**	
inlet U	82	82	[m/s]
inlet T	288	288	[K]
spray U	12.7	17	[m/s]

Mesh and simulation details		
Cell size	0.0005	[m]
Cell number	673816	
Time step	1e-07	[s]
Computational time	~100K	[s]

Looking at the spray behaviour in the two cases (Fig. (4)), since the inlet gas velocity is the same, the spray in the second case is expected to impact the wall at a lower distance from the nozzle with respect to case 1. This is due to the higher spray to gas momentum ratio in the second case. Looking at the spray, and at the diameter distribution, in figure 4 the diameter distribution at the beginning of the injection process is characteristic of column breakup, with a trail of smaller diameter parcels behind a core. As the injection progresses, it can be seen (see Fig.(4)) that an important part of the spray impacts on the filmer surface. Additionally it is possible to observe how the stripping of droplets at the corner of the plate is captured by the model. Looking at the data from the lower velocity case (case 1 from now on), the film heights obtained from the simulation were averaged in the direction perpendicular to the direction of the flow, and compared with the experimental results (see figure 5). This was done as the experimental data come from a measurment taken with optical techniques in a span-wise direction [1]. A good agreement with the experimental

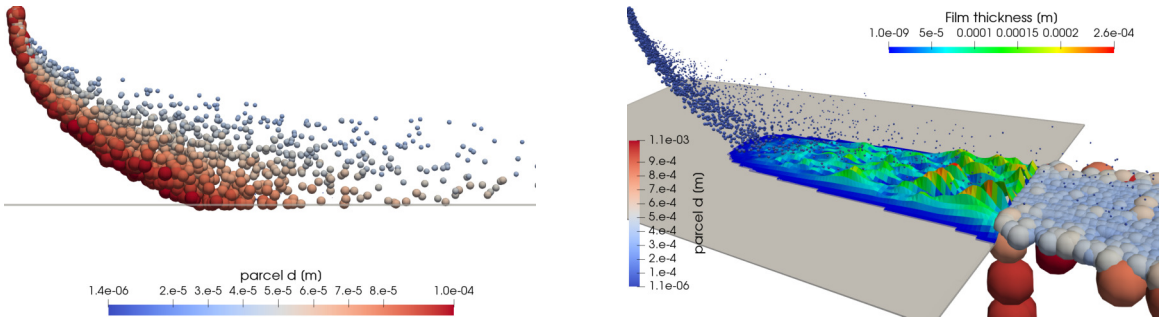

(a) (b)

Figure 4. Two snapshots taken from the simulation: (a) Taken at the beginning of the simulation (b) Snapshot with both spray and film thickness represented

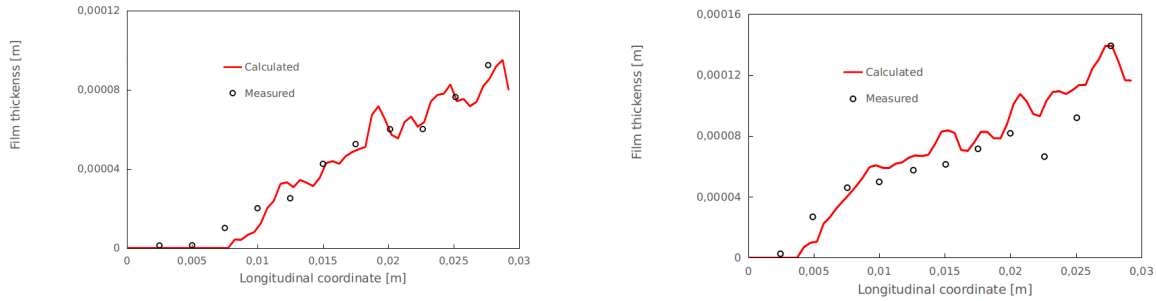

(a) (b)

Figure 5. Liquid film thickenss (a) Case 1 (b) Case 2

results can be seen for both cases, with the main discrepancies with respect to the experimental data being for low values of the distance along the filmer. These can be attributed to the spray/gas interaction, and they affect both cases, with a more noticeable effect for case 1.

Due to differential drag in the areas downstream of the spray, formation of thicker blobs can be noticed, that move along the surface, until they reach the edge of the filmer. The thickness of the film in this region is controlled by the stripping process, and as the injection process proceeds, dripping from the lower edge can be noticed, with the formation of droplets with a much higher diameter than the ones formed from the stripping from the upper edge. The formation and tracking of these droplets are important inside the SCR system, as they will evaporate more slowly and could reach the cayalyst surface. Furthermore, the persistence of this high thickness region near the edge represents a danger with respect to the deposit formation risk, and therefore the deployment of strategies that increment the stripping rate from the surface is required.

Transition case

To highlight the possibility of capturing the transition from dry to wet impact conditions, a case was set up, starting from a temperature higher than the wetting thresold.

For this simulation, all the data realtive to the type of interaction were registered as each parcel interacts with the filmer surface. In particular, the values of the thermal parameter T^* and of the ratio of the kinematic parameter to the critical kinematic parameter were evaluated to generate a map of the impingement regimes.
The evolution of the impacts is represented in figure (6). The data have been clustered in different time bins, and a transition from hot, destructive interactions to cold deposition and splash interactions can be seen. The quick transition from hot to cold interactions reflects the quick reduction in temperature experienced by the filmer surface. For the first clusters of impacts, an important number of parcels having a low value of the K/K_{crit} ratio can be noticed. These

parcels are the ones resulting from the thermal breakup interaction, that have a much lower value of the normal velocity with respect to the primary spray parcel, and therefore present a lower value of K. As the simulation progresses and the number of thermal breakup interaction reduces (as the region of direct spray impingement cools down below the threshold temperature) the number of these parcels reduces.

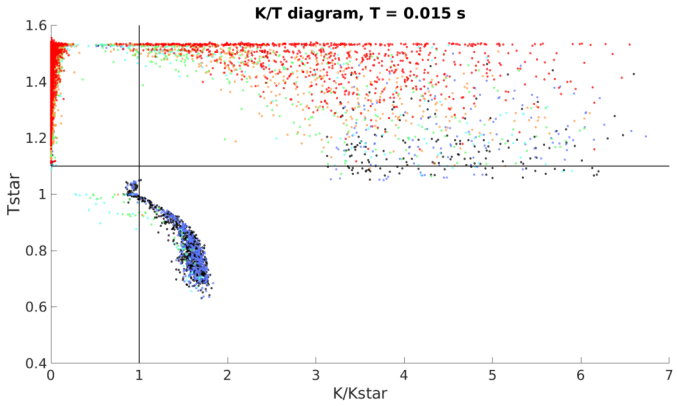

Figure 6. Impact regime map. The different colours represent the different time buckets, going from red (earliest impacts) to black (latest).

Conclusions

In this work, a CHT framework for the spray/wall interaction was developed and tested. This model was applied to a test case from the literature, comparing the results from the numerical simulation with the experimental data available. The difference in the impingement distance for the two different cases was captured in the simulations; furthermore, the values of wall film thickness were evaluated and compared showing good agreement with the the experimental data. Afterwards, to show the capabilities of the model to capture the transition from dry to wet impingement conditions, it was applied to a case with temperatures exceeding the wetting threshold. Data from the impingement of the parcels showed that the transition from dry to wet conditions is captured by the model.
Future developments of the model are necessary, to take into account the Leidenfrost effect, which limits the heat flux for high temperature applications. Finally, as the times required for deposit formation are much larger than the ones that can be simulated in a reasonable time using an unsteady solver, the development of a different framework for the simulation of the spray/wall impingement and related phenomena is required.

References

[1] Marco Arienti, L Wang, M Corn, Xiaolo Li, M.C. Soteriou, Tim Shedd, and Marcus Herrmann. Modeling wall film formation and breakup using an integrated interface-tracking/discrete-phase approach. *Journal of Engineering for Gas Turbines and Power*, 133:031501–7, 02 2013.

[2] Chengxin Bai and A. D. Gosman. Development of methodology for spray impingement simulation. *SAE Technical Paper, SAE International*, 950283, 1995.

[3] Baumgarten Carsten. *Mixture Formation in Internal Combustion Engine*. Springer, 2006.

[4] J.H. Ferziger and M. Peri. *Computational Methods for Fluid Dynamics*. Springer, 2002.

[5] H. Foucart, J. F. Le Coz C. Habchi, and T. Baritaud. Development of a three-dimensional model of wall fuel liquid film for internal combustion engines. *SAE International Journal of Engines*, 107, 1998.

[6] Dominik Kuhnke. *Spray/wall interaction modelling by dimensionless data analysis*. Shaker, 2004.

[7] C.H.R. Mundo, M. Sommerfeld, and C. Tropea. Droplet-wall collisions: experimental studies of the deformation and breakup process. *International journal of multiphase flow*, 940525:151173, 1995.

[8] Makoto Nagaoka, Hiromitsu Kawazoe, and Naomi Nomura. Modeling fuel spray impingement on a hot wall for gasoline engines. *SAE Technical Paper, SAE International*, 940525, 1994.

[9] Lorenzo Nocivelli. *CFD modeling and experimental characterization of urea/water solution injection inside SCR systems of diesel engines*. Ph.D. thesis, Politecnico di Milano, 2017.
[10] Akhtar S.W. and Yule A.J. Droplet impaction on a heated surface at high weber numbers. *ILASS-Europe*, page 37, 2001.
[11] Marshall W.R. Ranz W.E. *Internal Combustion Engine Modeling*. Hemisphere Publishing, 1952.
[12] Norbert Wruck. *Transientes Sieden von Tropfen beim Wandaufprall*. Shaker, 1998.